Environmental Science
Water Research & Technology

Accepted Manuscript

ROYAL SOCIETY OF CHEMISTRY

rsc.li/es-water

Acid-base dynamics in seawater reverse osmosis: experimental evaluation of a reactive-transport algorithm

Oded Nir*, Liron Ophek and Ori Lahav

Faculty of Civil and Environmental Engineering, Technion – IIT, Haifa, 32000, Israel;

*corresponding author, E-mail: odednir@campus.technion.ac.il

Abstract

Acid base properties such as pH, alkalinity and boron are essential components for the design and operation of seawater reverse osmosis desalination, influencing critical processes such as membrane scaling, biofouling and boron permeation. However, due to the high complexity of acid-base dynamics in both the retentate and permeate streams of reverse osmosis applications, the evolution of acid-base related properties in these streams is not yet completely understood. This often leads to overly simplified models resulting in inaccurate predictions, which may impede optimal design and thereby the cost-effectiveness of the process. This paper introduces a unique computerized model dedicated to modeling acid-base dynamics within seawater reverse osmosis processes based on a reactive-transport algorithm, which couples transport and equilibria phenomena. The *WATRO* (Weak Acid Transport Reverse Osmosis) simulation program based on this algorithm (freely available as ESI) is experimentally tested here and shown to extend the predictive capacity and accuracy for these important quantities beyond previous work, and also beyond the capabilities of available commercial software. Implications related to 1st and 2nd pass $CaCO_3$ scaling and boron rejection are exemplified and discussed. From the practical standpoint, the advantages of the suggested approach are particularly prominent for 2nd RO pass modeling and design, mainly due to the passage of hydronium and hydroxide ions through the membrane.

Water Impact

Reverse osmosis technology for seawater desalination is considered by many as the best available solution for water scarcity. Acid-base species naturally occurring in seawater have significant implications on process design, however while the rejection of salts could be predicted with reasonable accuracy by available simulation algorithms, predicting the behavior of partially ionized acid-base species has been thus far beyond reach. Here we describe a simulation tool specifically aimed at predicting acid-base dynamics in seawater reverse osmosis. This algorithm is shown to produce considerably improved projections of process parameters related to agricultural uses and chemical scaling, allowing for a more cost-effective process design. Fundamental understanding of pH variations and pH dependent processes during RO filtration is stimulated by this study.

1. Introduction

Weak acid species appear in seawater at low concentrations relatively to major seawater ions. Nevertheless, these species significantly affect the design and cost of most SWRO (seawater reverse osmosis) applications. The two major weak-acid systems in seawater are the carbonate system (~2.3 mM) and the borate system (~0.46 mM). The carbonate system is important mainly due to $CaCO_3$ scaling propensity, which may limit the recovery ratio and require the addition of antiscalant chemicals[1,2,3]. The boron system is important due to the detrimental effect of this species at low concentrations on plants, which may limit the use of desalinated water for agriculture and urban gardening[2]. Both weak acid systems comprise of several species having the propensity for association or dissociation of H^+ or OH^-. The relative concentration of each species, including H^+ and OH^-, is a result of the acid-base state of equilibrium, which depends on temperature, pressure and solution composition.

Each carbonate and borate species is characterized by a unique protonation state and electric charge within its own weak-acid system, resulting in radically different permeation rates through RO (reverse osmosis) membranes for different carbonate and borate containing species[4,5]. Therefore, the two main challenges in modeling the transport of weak-acid species in RO are: (1) determining the feed-side concentration of these species using a suitable speciation model; (2) determining the trans-membrane flux of all species using a suitable physical transport model. Simulation of practical RO applications, requiring significant permeate recovery from source water (recovery ratio) is particularly challenging, since concentrating the feed by increasing permeate recovery invariably changes the acid-base equilibria (indicated by a change in pH) of the rejected solution[6,7].

In our previous works we introduced a coupled modeling approach which takes into account the evolution of pH throughout the passage of the brine in the membrane train, by evoking elaborated chemical speciation model at each infinitesimal permeate recovery increase[8,9]. For the purpose of calibration and experimental validation of the coupled approach a new self-consistent method for measuring pH in SWRO brines was developed[10]. Furthermore, initial model validation experiments described in that study[10] revealed the influence of H^+ and OH^- transport on acid-base dynamics in RO. This issue was addressed in a recent study, in which semi-analytical equation based on the diffusion-electromigration theory was derived and fitted to experimental results[11]. In the current paper, findings from our previous work are incorporated into a computer code termed *WATRO* (Weak Acids Transport in Reverse Osmosis), an advanced simulation program for pH, alkalinity and boron dynamics, that can be utilized for the design and operation of the 1st and 2nd RO steps typically employed in SWRO facilities. The predictive capacity of *WATRO* towards pH, alkalinity and boron is tested here by comparing simulated predictions to experimental pilot results obtained at realistic recovery ratios and various operational conditions.

2. Description of the simulation code

The simulation code, written in the programming language Python[12] (v2.7), executes the membrane-transport and the mass balance equations required for the model, while chemical speciation calculations, osmotic coefficients and solution densities are obtained from PHREEQC[13]. The two programs are coupled, i.e. information is automatically exchanged between them, enabling detailed and comprehensive chemical-equilibrium modeling at each iterative step. Coupling PHREEQC to Python is relatively easy thanks to efforts made by the creators of PHREEQC in USGS to develop free modules used specifically for this purpose[14]. Featuring the

numeric engine and thermodynamic database of PHREEQC, these modules (also called COM objects) are operated from within the Python environment using pre-determined keywords. Typically, over a thousand calls are made to the function running the PHREEQC module during a simulation run of a full scale SWRO process, while the runtime is typically below one minute (Processor: Intel®'s i5-3317U, 1.7GHz; 4GB RAM). The code was written for SWRO applications however it is theoretically valid for the general case of multi-ionic solutions, with NaCl as the dominant salt[15], and the carbonate system and borate system as the only weak-acid systems apart from the water dissociation products.

2.1. Permeate flux and salt concentration

As a preliminary step for the weak-acids model the code initially predicts the permeate volumetric flux (J_V) and the salt concentrations in the bulk water, unstirred layer and permeate solutions. These are calculated for each numerical recovery segment, using the solution-diffusion-film model [16,17] and saved in arrays for later use. It is assumed at this stage that the concentration of the weak-acid species is relatively small and thus their contribution to the osmotic pressure of the bulk solution can be neglected. Also applied is the common assumption that seawater salt permeation can be modeled via a single permeability coefficient (P_s) without significant loss of accuracy. For modeling purposes it was assumed that Na^+ and Cl^- are the only major seawater ions permeating through the membrane; a reasonable assumption for SWRO. A detailed description of this sub-algorithm is shown in the ESI file (section 2). Coupling the transport simulation to PHREEQC has the added value of obtaining the osmotic coefficient for every water composition through the use of the Pitzer[18–20] model embedded in the software[21,22] (providing that the components are included in the thermochemical database), which enables a more accurate calculation of the osmotic

pressure and thus of the permeate flux[23–25]. The density of the solution is also calculated by PHREEQC, which is useful for estimating the mass transfer coefficient[22,23].

2.2 Weak acid reactive transport

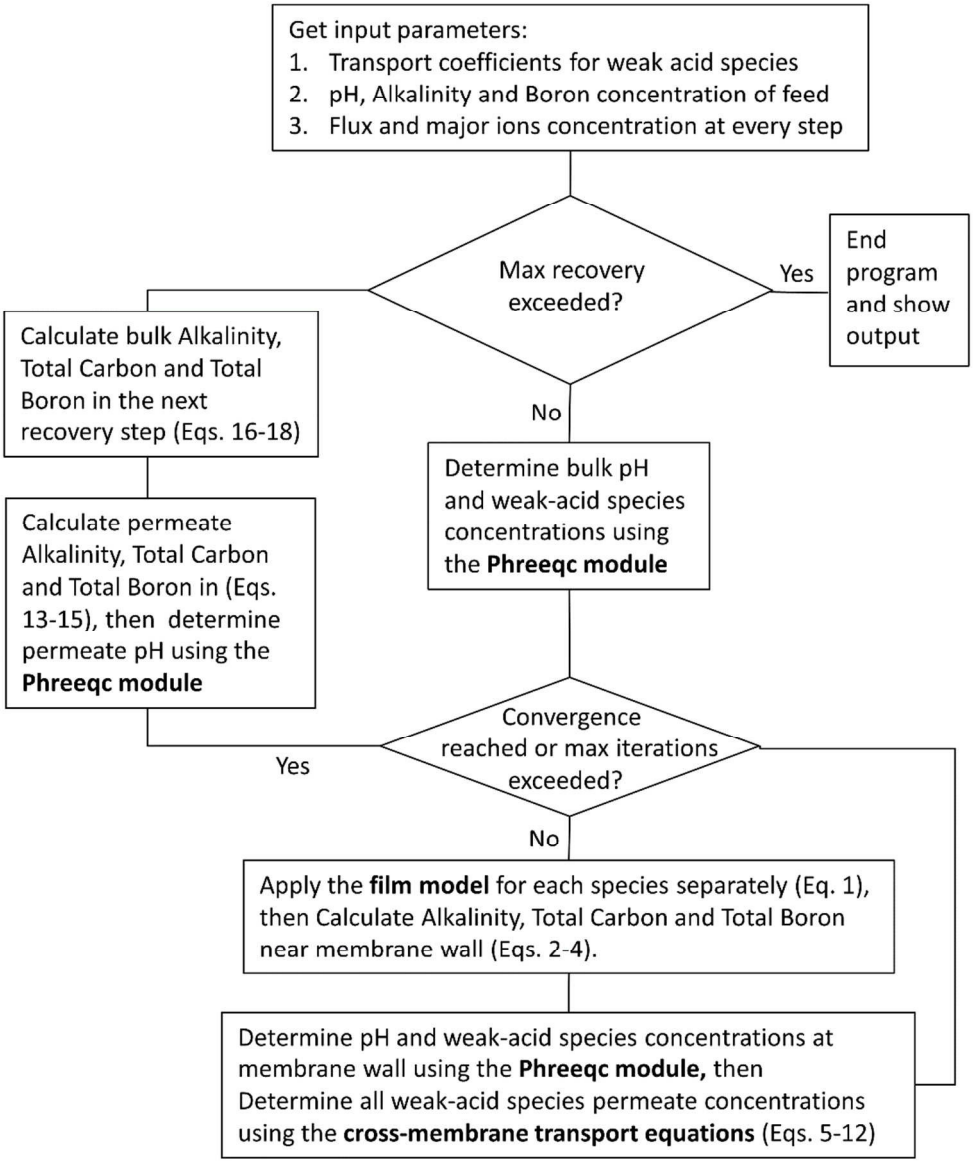

Figure 1. A flow diagram of the reactive transport algorithm underlying the WATRO (weak acid transport in reverse osmosis) simulation code (see ESI†).

Once the water flux and major ion composition in the bulk water, film layer and permeate are known for each numerical recovery segment, the weak acid reactive-transport simulation is initiated, following the algorithm described in Fig. 1 and the transport equations shown in Table 1. As seen in Fig. 1, speciation of the bulk by the PHREEQC module is performed once for every recovery step. Subsequently, the acid base properties of both the film layer and the permeate are determined by an iterative procedure, which converges once the acid-base equilibria in the film layer, i.e. species concentrations received from the speciation made by the PHREEQC module, is in close agreement with the equations for concentration-polarization (Eq. 1), proton and species mass balance in the film layer (Eq. 2-4) and membrane transport (Eq. 6-12). The transport of boric acid, borate and bicarbonate species is described by the solution-diffusion model, while for dissolved carbon-dioxide and carbonate ion, rejections of 0%[4] and 100% respectively are assumed. The transport of hydronium and hydroxide ions is described by an approximate analytical solution (Eqs. 10-13 in table 1) for the phenomenological Nernst-planck equation. Eq. 10, which was developed and validated in[11], considers both diffusion and electromigration which was found to significantly affect the pH and alkalinity of the solutions both in the permeate [refs] and in the feed side (see Results section). The parameter θ appearing in Eq. 10 and defined in Eq. 13 is a function of pH and salt concentration. For modeling purposes, an empirical correlation for θ was derived based on data from[11]. A description of the correlation and graphical depiction of the fitting are given in the EIS file (Section 5, Fig. 5S).

The permeability constant for boric acid (P_B), shown in Eq. 5, could be either received as direct input (when it is obtained from the literature or determined from independent experiments as done in this work) or estimated based on manufacturer's published boron rejection performance. The permeability constants for the borate and bicarbonate monovalent ions within the solution-

diffusion mechanism were assumed equal to the overall salt permeability (P_s). It is noted that electromigration, which is neglected here for these species also contributes to their transmembrane fluxes, however for RO this simplifying assumption is expected to have a negligible effect on the total alkalinity, boron and inorganic carbon fluxes which are (when occurring at significant magnitudes) dominated by H^+/OH^-, $B(OH)_3$ and CO_2 respectively. For charged weak-acid species, the mass transfer coefficient (k_j) appearing in Eq. (1) is assumed identical to the average mass transfer coefficient of salt, which can be either provided by the user or estimated by the program (see section 3 of the ESI file for further information). The mass transfer coefficient of the uncharged $B(OH)_3$ k_B is also provided by the user or estimated to be twice the magnitude of k_s (see section 4.1 for explanation).

After all individual species permeate concentrations are determined, the permeate alkalinity, total boron and total inorganic carbon concentrations are computed (Eqs. 15-16). This enables the calculation of both the permeate pH (by the PHREEQC module) and the bulk alkalinity, total boron and total inorganic carbon concentrations in the next recovery step (Eqs. 17-19). The algorithm continues to run until the desired recovery is reached. pH, alkalinity and boron concentrations are recorded for every recovery step, thus the evolution of this acid-base related quantities throughout the desalination can be evaluated and compared to experimental results.

Table 1 – Equations used in the WATRO (ESI†) simulation program

Estimation of weak-acids species concentration ($C_{WA,j}$) in the film layer
$C_{WA_j,m,i} = C_{WA_j,p,i} + (C_{WA_j,b,i} - C_{WA_j,p,i})\,\mathrm{e}^{J_{v,i}/k_{j,i}}$ (1)
Weak acid species mass balance in the film layer
$B_{T,m,i} = C_{B(OH)_3 m,i} + C_{B(OH)_4^- m,i}$ (2); $C_{T,m,i} = C_{CO_3^{2-} m,i} + C_{HCO_3^- m,i} + C_{H_2CO_3^* m,i}$ (3)
Alkalinity mass balance in the film layer
$Alk_{m,i} = 2C_{CO_3^{2-} m,i} + C_{HCO_3^- m,i} + C_{B(OH)_4^- m,i} + C_{OH^- m,i} + C_{MgOH^+ m,i} - C_{H^+ m,i} - C_{HSO_4^- m,i}$ (4)

Permeate concentrations of boron species

$$C_{B(OH)_3\,p,i} = P_B C_{B(OH)_3\,m,i} / (J_{v,i} + P_B) \quad (5); \quad C_{B(OH)_4^-\,p,i} = P_s C_{B(OH)_4^-\,m,i} / (J_{v,i} + P_s) \quad (6)$$

Permeate concentrations of carbonate species

$$C_{H_2CO_3^*\,p,i} = C_{H_2CO_3^*\,m,i} \quad (7); \quad C_{HCO_3^-\,p,i} = P_s C_{HCO_3^-\,m,i} / (J_{v,i} + P_s) \quad (8); \quad C_{CO_3^{2-}\,p,i} = 0 \quad (9)$$

Permeation of alkalinity due to H^+/OH^- Diffusion-Electromigration

$$\Delta Alk_{p,i} = \frac{C_{OH^-\,m,i}\omega^*_{OH_i}}{\omega^*_{OH}(1-R_{s,i})^{\theta,i} + J_{v,i}\dfrac{1-(1-R_{s,i})^{1+\theta_i}}{R_{s,i}(1+\theta_i)}} - \frac{C_{H^+\,m,i}\omega^*_H}{\omega^*_H(1-R_{s,i})^{-\theta_i} + J_{v,i}\dfrac{1-(1-R_{s,i})^{1-\theta_i}}{R_{s,i}(1-\theta_i)}} \quad (10)$$

$$\omega^*_{OH^-} = \omega_{OH^-} + \omega_{H^+} C_{H^+} / C_{OH^-} \quad (11); \quad \omega^*_H = \omega_{H^+} + \omega_{OH^-} C_{OH^-} / C_{H^+} \quad (12); \quad \theta = \frac{p_{Na^+} - p_{Cl^-}}{p_{Na^+} + p_{Cl^-}} \quad (13)$$

Weak-acid species mass balance in the permeate

$$B_{T,\mathrm{p},i} = C_{B(OH)_3\,\mathrm{p},i} + C_{B(OH)_4^-\,\mathrm{p},i} \quad (14); \quad C_{T,\mathrm{p},i} = C_{\mathrm{HCO_3^-}\,p,i} + C_{H_2CO_3^*\,p,i} \quad (15)$$

Alkalinity mass balance in the permeate

$$Alk_{\mathrm{p},i} = C_{\mathrm{HCO_3^-}\,p,i} + C_{B(OH)_4^-\,p,i} + \Delta Alk_{p,i} \quad (\Delta \mathrm{Alk_p} \text{ as appears in Eq. 10}) \quad (16)$$

Boric acid, Carbonate and Alkalinity mass balance

$$B_{T,b,i+1} = [B_{T,b,i}(1-r_i) - B_{T,p,i}\,\mathrm{dr}] / (1-r_{i+1}) \quad (17)$$

$$C_{T,b,i+1} = [\mathrm{C}_{T,b,i}(1-r_i) - C_{T,p,i}\,\mathrm{dr}] / (1-r_{i+1}) \quad (18)$$

$$Alk_{b,i+1} = [\mathrm{Alk}_{b,i}(1-r_i) - Alk_{p,i}\,\mathrm{dr}] / (1-r_{i+1}) \quad (19)$$

3. Experimental

RO experiments were carried out using a membrane filtration pilot-scale unit, supporting one 4X40" membrane module (diameter = 4", length = 40"). A schematic description of the experimental setup is given in Fig. S1 in the ESI file. In all the filtration experiments, feed water was pumped from the feed tank to a high-pressure positive-displacement pump (Hydra-Cell, D/G-10-X), using a centrifugal booster pump (Pedrolo, 2-4CR). The pressurized feed water flowed through the membrane element, placed inside a pressure vessel (Bell, ORL4-E-1000), resulting in brine and permeate streams. The working pressure was controlled by a valve at the brine outlet,

while the feed flow-rate (cross-flow velocity) was independently adjusted using a frequency converter. Both pressure and cross-flow velocity were continuously recorded by digital meters connected to a computer and the values reported here are the averages of the feed and brine streams over 3-5 minutes. Permeate flow rate was measured volumetrically. Brine temperature was maintained at 25 ± 1^0C by a titanium plate heat exchanger and a chiller (capacity: 9000 kcal/h). The experiments for determining transport constants (Table 2) were conducted at low recovery (i.e. at full recirculation mode when both brine and permeate streams are circulated back to the feed tank) and low pH (6.2-6.5), where >99% of dissolved boron is in the form of $B(OH)_3$. The feed was real Mediterranean seawater in the cases where seawater membranes were used and simulated 2^{nd} pass feed water (i.e. 1^{st} pass permeate) when brackish RO membranes were applied. Feed water ionic compositions for these experiments can be found in the ESI file. Transmembrane pressure, flux, salt and total boron concentration were recorded and analyzed as described in the ESI file.

The model evaluation experiments were conducted at high recovery ratios. Permeate was collected in a different tank until the desired recovery achieved. Once the desired recovery was attained the permeate was directed back to the feed tank and allowed to stabilize for 20 minutes before measurements were taken (pressure, flux, pH, temperature) and samples collected. Samples were taken from all streams at selected recovery points and were measured for pH (the method described in[10] was used for concentrated solutions), alkalinity (using the Gran titration method), boron and major ions (ICP-AES). All reported concentrations represent the sum of all major ions appearing in seawater. Feed compositions for the validation experiments are provided in Table 2.

Table 2. Composition of feed solutions used in the model evaluation experiments. All concentrations are in mg/l. Alkalinity is given in mg/l as $CaCO_3$.

Membrane	pH	Cl^-	Na^+	Mg^{2+}	SO_4^{2-}	K^+	Ca^{2+}	Alkalinity	B_T
SWC6	9.35	20106	11432	1285	3248	433	412	36.8	4.22
SW30HRLE	8.59	14872	8610	934	2744	311	344.5	154.8	3.62
SW30HRLE	8.24	16580.143	9573	1044	3071	367	397	120	3.670
ESPA2	9.62	447.7	292	3.33	16.5	-	-	12.66	2.16

4. Results and Discussion

4.1. Transport parameters

Prior to the model evaluation experiments, the transport constants required by the solution-diffusion-film model were determined via separate filtration experiments for each membrane element used in this work. Permeate flux and solutes concentrations data (Table S1 in the ESI file) were recorded for varying transmembrane pressure and used to calculate the mass transfer coefficients (k) and the permeability coefficients (P) for boric acid and for the dissolved salt (a single set of coefficients, k and P, was used as an overall effective average for all charged solutes). For boric acid, the transport constants were determined by non-linear optimization, while for the salt, linear regressions were used, following the logic of the osmotic-pressure method[26]. Detailed information on the calculation of the coefficients is found in the ESI file (section 3).

Table 3. Experimental transport parameters used as input for the *WATRO* model evaluation.

	P_w (m/s/bar)	P_{salt}(m/s)	k_{salt}(m/s)	$P_{B(OH)3}$(m/s)	$k_{B(OH)3}$(m/s)
SW30HRLE	4.89E-07	2.90E-08	1.05E-05	2.06E-06	2.57E-05
SWC6	5.79E-07	1.94E-08	2.32E-05	1.88E-06	1.00E-03*
ESPA2	1.27E-06	9.40E-08	9.40E-06	2.78E-05	1.62E-05

*Assumed value due to experimentally insignificant concentration-polarization for boric acid (see text for further explanations)

The transport constants shown in Table 3 correspond to the solution-diffusion-film model. It is generally accepted that this model provides a good approximation for salt transport in RO[17].

Regarding boric-acid however, several recent publications[27,28] used the Spiegler-Kedem-film model (see Eq. S10 in the ESI file) which couples boric-acid permeation to that of water (often viewed as convection). The coupling is expressed by the parameter σ which ranges from 0 (in the case of full coupled flow) to 1 (in case of no coupling). In this work however, when transport constants were fitted to the results according to the Spiegler-Kedem-film model the optimization yielded $\sigma_{B(OH)3}$ values which were very close to unity (>0.999), as assumed in the solution-diffusion-film model, while the other model parameters, $P_{B(OH)3}$ and $k_{B(OH)3}$ were very similar for both models, suggesting that boric-acid transport can be fully explained by the solution-diffusion-film mechanism. This observation is in accord with recent theoretical and empirical evidence which support the premise of negligible convection for today's extremely thin RO membranes[11,29]. The salt permeability (P_{salt}) was smaller by ~2 orders of magnitude than the boric-acid permeability ($P_{B(OH)3}$) for all the membranes used. As expected, the water permeability was the highest for the ESPA2 brackish water membrane, followed by the SWC6 high-flux seawater membrane and the lowest for the SW30HRLE seawater membrane. The latter membrane was two years old and deteriorated as a result of demanding lab use, which may explain its higher permeabilities for salt and boric-acid, compared to the new SWC6 element.

Surprisingly, the mass transfer coefficient obtained for the salt was significantly smaller than the one found for boric-acid ($k_{B(OH)3}$), despite the fact that the diffusion coefficient in water found in the literature is lower for the latter. This implies a higher tendency of charged solutes towards concentration polarization, which may be explained by electrostatic interactions of ions with the charged membrane surface or with the fouling layer, by ion-ion interactions, or by any combination of the three. Although beyond the scope of this work, this finding calls for further research, aimed at understanding the role of electrostatic interactions in concentration-polarization

occurring during RO filtration. $k_{B(OH)3}$ for the SWC6 membrane converged to a very large number, suggesting negligible concentration-polarization for boric acid. Since $k_{B(OH)3}$ could not be accurately determined by the non-linear fitting method in this case, the value shown in Table 3, which is sufficiently large for making concentration-polarization practically insignificant, was used as input for the relevant model run.

4.2. Model evaluation and dominant processes affecting pH, alkalinity and boron

RO filtration experiments were conducted and compared to model prediction. Operational conditions closely simulated the decrease in permeate flux and the increase in the retentate concentration, as encountered in actual SWRO applications. Real seawater or synthetic 1st pass permeate (2nd pass feed) were used as feed water in these experiments. Measured water flux and salt concentration values were reasonably well predicted by the *WATRO* program for all experiments (see Fig. 4S on the ESI file), with errors typically below 10%. This is critical for the purpose of model evaluation since water flux and salt concentration affect the pH, alkalinity and boric acid values.

4.2.1. SWRO 1st pass evaluation experiments

Predictions made by the simulation program for the 1st SWRO pass were compared to experimental results at three different feed pH values and for two different membranes. When the SWC6 high-flux membrane was used, the seawater feed was pre-treated by acid-stripping[2,30] to remove most of the carbonate system and adjusted to pH 9.35. As shown in Fig. 2, the predicted concentrate pH closely matched the measured values for all experiments, with errors typically <0.1 pH units. Experimental permeate pH values were also predicted reasonably well, apart from the results obtained at high recovery at feed pH 8.24. It is noted that 1) the permeate pH is highly

unstable due to the low buffer capacity of the solution and thus a small error in model calculations of e.g. CO_2 permeation may lead to high errors, and; 2) The parameters used in Eq. 10, describing H^+/OH^- permeation, were determined only for the ESPA2 RO membrane. Nevertheless, the model was successful in predicting most of the experimental points, which demonstrates its robustness. A decrease in concentrate pH with the recovery ratio was recorded for feed pH values >8, as previously observed[10,31]. In contrast, at feed pH of 7 the trend is reversed and the concentrate pH increases with recovery, as predicted by the model (see Fig. 2) and was recorded in previous works[4,32,33]. Correspondingly, at feed pH 7 the permeate pH is lower than the feed pH, while at feed pH>8 the permeate pH is higher.

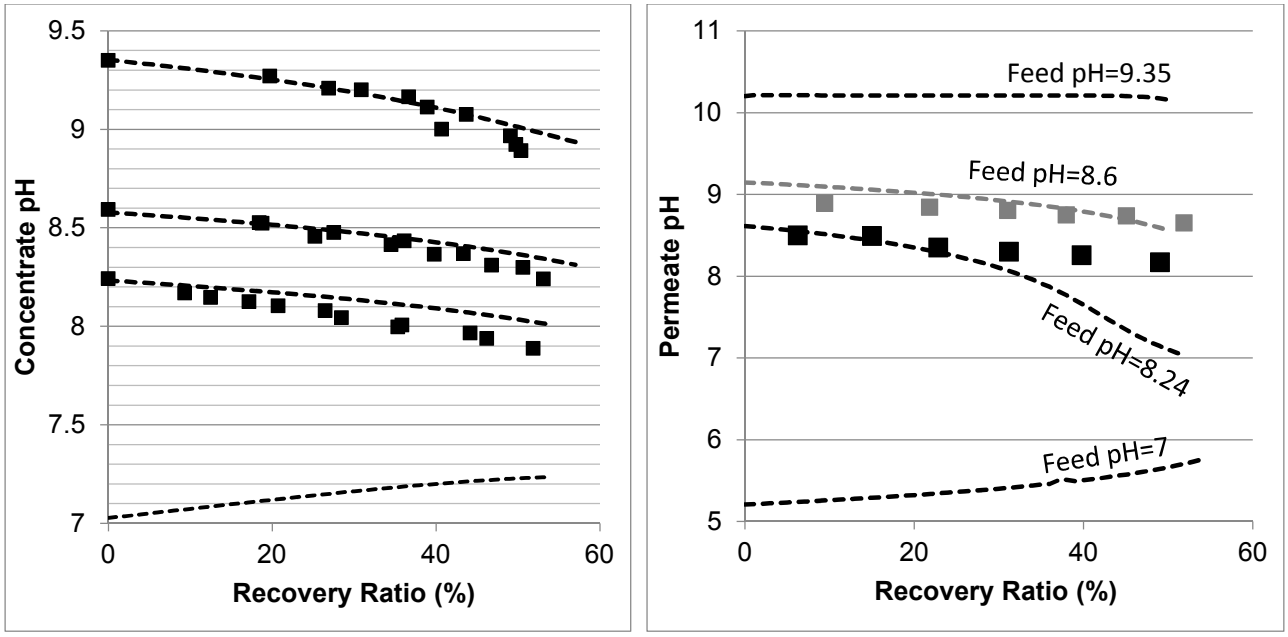

Figure 2. Evolution of concentrate (left graph) and permeate pH as a function of the recovery ratio. Square markers represent experimental results. Dashed lines are model predictions. Membranes used were Dow's SW30HRLE (for feed pH 8.24 and 8.6) and Hydranautic's SWC6 (for feed pH 9.35).

In order to understand the evolution of pH, alkalinity and boron values within high recovery RO, transport-equilibria processes affecting acid-base dynamics need to be known. These could be classified into processes which increase concentrate pH and processes which decrease it. pH increase could be induced by permeation of weak acids, (i.e. CO_2 and $B(OH)_3$ in the case of seawater) and of H^+ ions. pH decrease is the result of weak bases (HCO_3^- and $B(OH)_4^-$) and OH^- permeation (which may be coupled to reverse flux of H^+ ions[11]) and the increase of salt concentration and ionic strength, which reduces the activity of the negatively charged weak bases. By examining the experimental results and by using the model, the dominant transport-equilibria process for every process scenario can be revealed. The decline of retentate pH with recovery at feed pH>8 indicates that pH increasing processes are overwhelmed by pH decreasing processes.

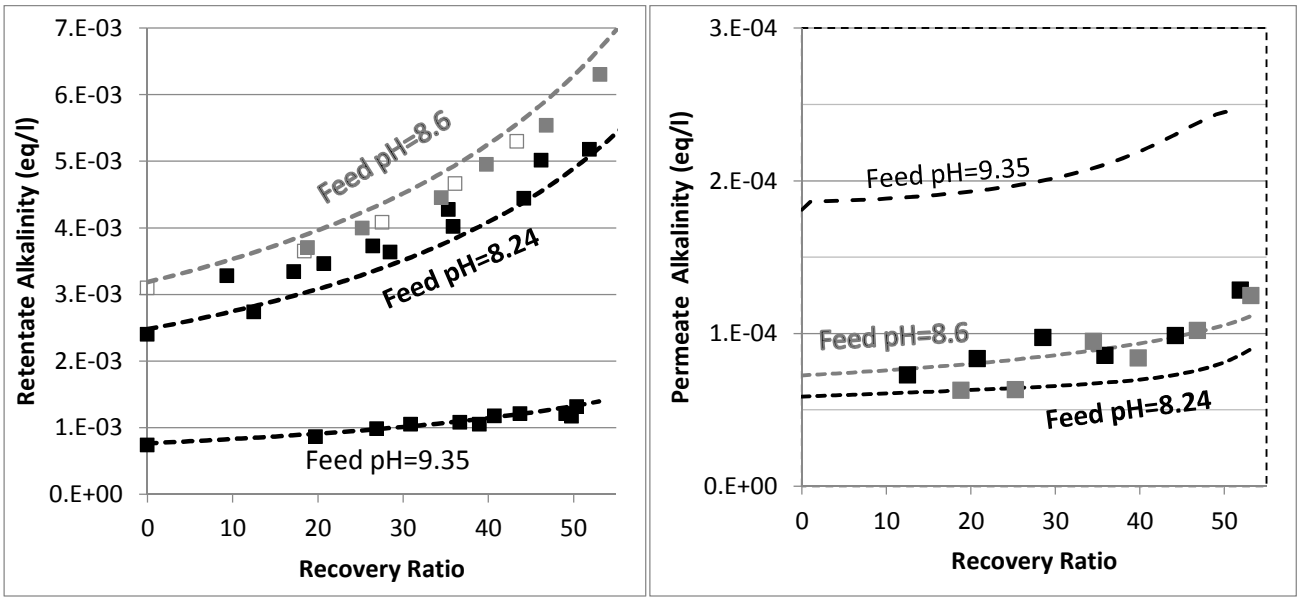

Figure 3. Evolution of retentate (left hand graph) and permeate alkalinity as a function of recovery ratio. Square markers are experimental results. Dashed lines are model predictions.

Determining which pH-changing process is dominant can be deduced from the measured and modeled alkalinity values shown on Fig. 3. At feed pH 8.24 and 8.6 the alkalinity concentration

was doubled at 50% recovery implying that alkalinity-comprising species were almost fully rejected. Correspondingly, the permeate alkalinity measured and modeled for these experiments was almost two orders of magnitude lower than in the retentate. Among the pH decreasing processes, the increased ionic strength in the retentate is the only one which does not involve alkalinity transfer from the retentate to the permeate; therefore it is most likely the main reason for pH decrease in this case. In contrast, for feed pH 9.35, the permeate alkalinity was higher even though feed alkalinity was lower due to the decarbonation pretreatment, suggesting that H^+/OH^- permeation dominantly affect the retentate pH in this case. This is in par with the high permeate pH predicted for feed pH 9.35 (see Fig. 2), which is the result of H^+/OH^- electromigration.

The mechanisms underlying pH evolution for each case were further inspected by using a modified version of *WATRO* in which the function adjusting for H^+/OH^- transport is switched off. When this is performed for the feed pH 9.35 case, the predicted pH of the retentate at 50% recovery becomes pH9.25, which is higher than the pH 9 value predicted by the fully functional model (and also measured), while the predicted permeate pH was lower (pH7.5-8 compared to pH10-10.2). Accordingly, the predicted permeate alkalinity was two orders of magnitude lower, while the retentate alkalinity at 50% recovery was doubled. Applying the same procedure for the case of feed pH 8.24 yielded a predicted pH value of 8.07 at 50% recovery, only slightly higher than the value predicted by the fully functional *WATRO* (8.03), while the permeate pH in this case dropped to 6.2-6.5 (compared to 8.1-8.6). Accordingly, the alkalinity in the retentate was almost unchanged while the permeate alkalinity dropped by ~50 μeq/l. These results suggest that for the case of high feed pH and low alkalinity, OH^-/H^+ electromigration is the dominant mechanism driving pH evolution in both the retentate (although the increase of salt concentration also plays a significant role for the retentate) and the permeate. For the case of seawater feed at ambient pH

and alkalinity, pH evolution in the retentate is almost exclusively controlled by the salt concentration while the pH of the permeate is determined mostly by OH^-/H^+ electromigration.

As seen in Fig. 4, the model accurately predicted the boron permeate concentrations at 50% recovery ratio for the three feed pH values and two membranes applied in the experiments (permeate boron concentrations were well predicted for most of the recovery range as shown in Fig. 6S in the ESI file). For the purpose of quantifying the effect of acid-base dynamics and pH evolution on boron permeation in the 1st SWRO step, a modified version of *WATRO* in which the concentrate pH remained unchanged in the retentate stream from the feed to the final concentrate was used. This assumption is evidently untrue[10], nevertheless it is applied in most full-scale boron transport models published in the scientific literature[34–36].

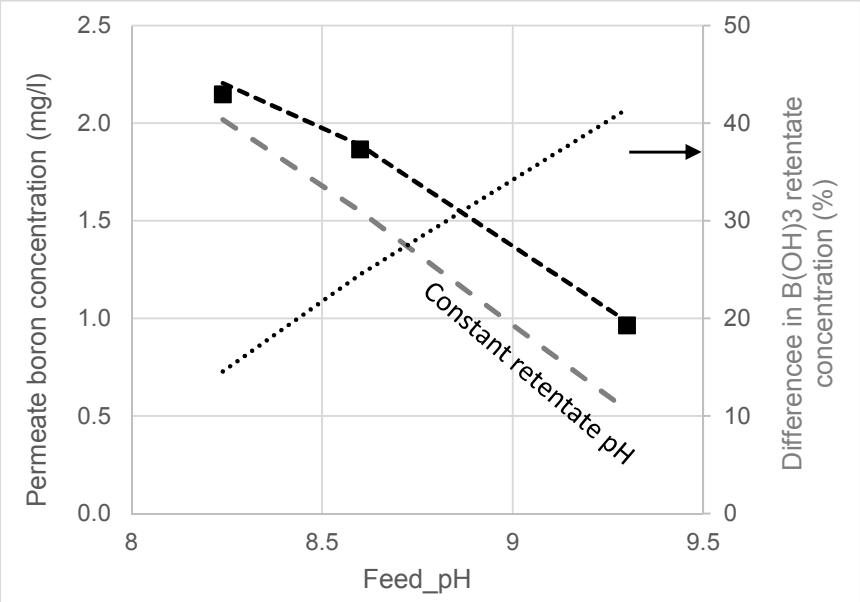

Figure 4. Boron permeate concentrations at 50% recovery at varying feed pH. Symbols represent experimental results. Dashed lines are model projections by the fully functional *WATRO* (black) and the modified version in which the retentate pH is constant (grey). The dotted line shows the relative difference in $B(OH)_3$ concentrations projected by the two models.

Examining the comparison between the two versions of the model presented in Fig. 4 it can be seen that predictions made by the modified constant-pH model are similar to the fully-functional model at feed pH 8.24. However, as the pH increases, predictions for the constant pH assumption significantly differ from the fully-functional model and from experimental results. The reason for this effect, also depicted in Fig. 4, is the increasing difference in the projections of $B(OH)_3$ retentate concentration at 50% recovery made by the two versions of *WATRO*. Although the decline in pH is similar for feed pH 8.24-9.35 (see Fig. 2), the underestimation of the (poorly rejected) $B(OH)_3$ concentration by the constant pH assumption is more apparent when the pH is high and $B(OH)_3$ concentration is low. Therefore, although SWRO boron-transport models which assume constant pH may produce reasonable predictions at feed pH<8.3, they are unreliable at higher feed pH. It is therefore recommended that a more generic model, as the one suggested here, will be used to explore the interesting prospect of operating the 1st SWRO pass at high pH [30,37].

4.2.2. SWRO 2nd pass evaluation experiments

Predictions made by the *WATRO* simulation program were further compared to 2nd pass experimental results. Recovery ratio of 86% was obtained in this experiment with ESPA2-4040 membrane element, commonly used for this purpose. The feed pressure was 11 bars, while the feed pH was 9.6. In contrast to the 1st pass retentate which contained weak-acid systems in significant concentrations, the 1st pass permeate (which is the feed for the 2nd pass) is poorly buffered. As a result, both the retentate and permeate pH boron and alkalinity are highly affected by H^+/OH^- trans-membranal flux, which induce a decline in retentate pH as the recovery increases. As shown in Fig. 5, the evolution of pH in both retentate and permeate streams was well predicted. However when H^+/OH^- permeation is switched off, the retentate pH evolution assumes an opposite

trend, differing from the experimental results by >1.5 pH units at high recovery ratios. The manufacturer software's prediction agrees with this simulation run, as they both falsely assume that permeation of $CO_{2(aq)}$ and $B(OH)_3$ solely determines the retentate pH in the 2nd pass. Similarly, H^+/OH^- permeation also controls the permeate pH in the 2nd pass as is implied from the results shown in Fig. 5. When this function is switched off the predicted permeate pH becomes lower than that in the retentate and increases with the recovery ratio, which is in good agreement with the manufacturer's design software. In contrast, the fully functional model predicted higher permeate pH and a pH value decreasing with recovery, which is in better agreement with the experimental results.

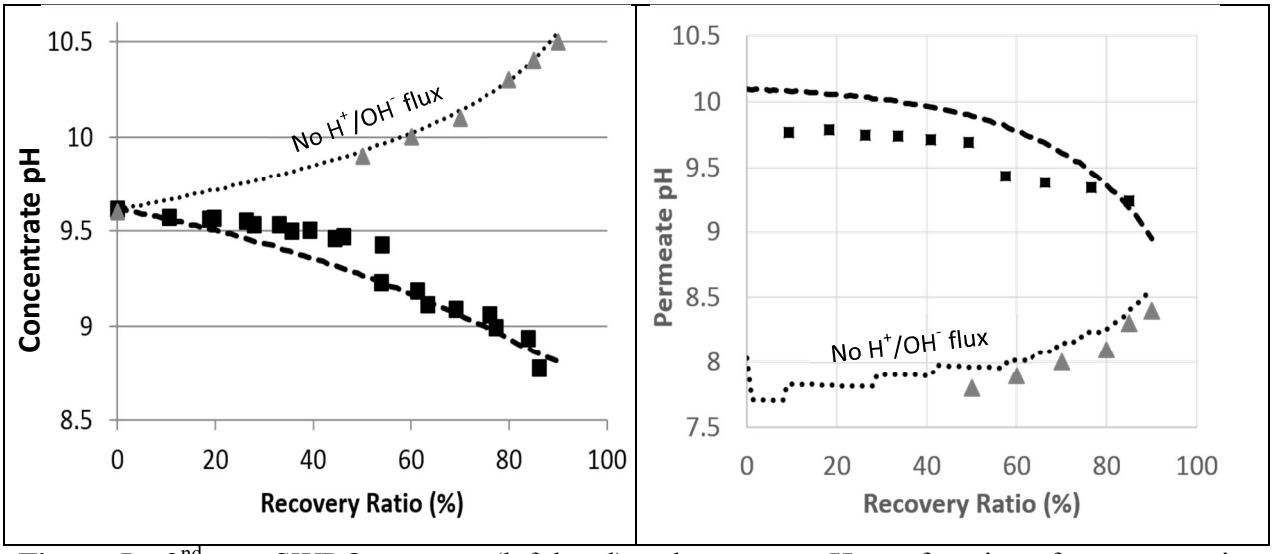

Figure 5 – 2nd pass SWRO retentate (left hand) and permeate pH as a function of recovery ratio. Squares represent experimental results. Dashed lines are the projections by the fully functional *WATRO* model. Dotted lines are simulation results made by the modified version of *WATRO* with no H^+/OH^- flux. Triangle markers are projections made by the membrane manufacturer's process design software.

Predicted and measured boron concentrations in the 2nd pass permeate are shown in Fig. 6. The results suggest that modeling the pH evolution correctly dramatically improves the accuracy of

model predictions for boron concentration in the 2nd pass permeate. While the fully functional model accurately predicted boron permeate concentrations, the simulation run without H^+/OH^- flux significantly underestimated boron permeate concentrations, especially at high recovery ratios. This underestimation, which was in agreement with the manufacturer software, is a result of the over predicted retentate pH leading to underestimated $B(OH)_3$ retentate concentration. The claim that the manufacturer's software failed due to incorrect treatment of acid-base dynamics at high feed pH is supported by the simulated results at feed pH 7, where changes in the retentate pH (by as much as 1 pH unit, which is normally not expected) do not significantly affect boron speciation. The good agreement between the *WATRO* code and the manufacturer design software, suggest that $B(OH)_3$ permeability and transport are treated similarly, however *WATRO* is more general and may be used for high feed pH, which is the common practice in the 2nd pass. These results demonstrate the practical significance of the suggested approach towards simulating 2nd pass results, which is often aimed mainly at boron removal.

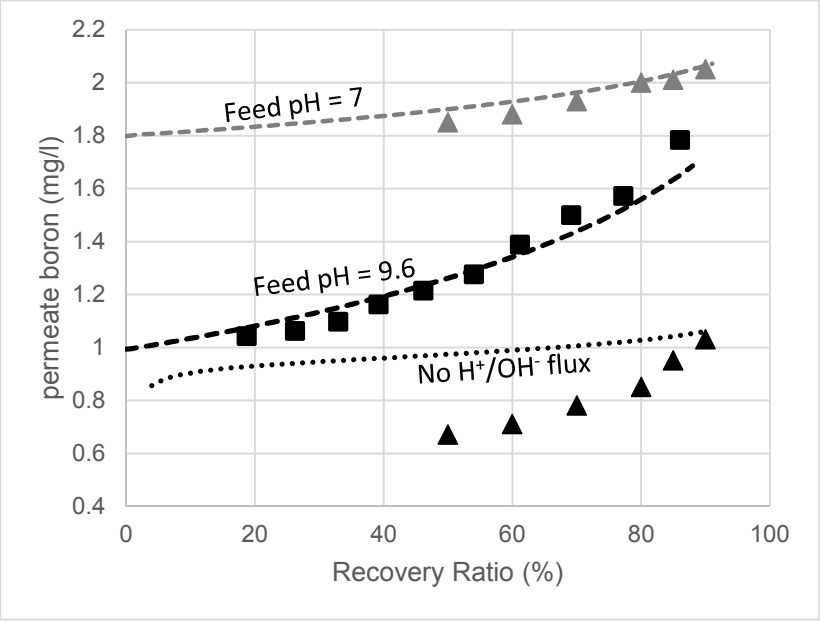

Figure 6 - Boron permeate concentrations of 2nd SWRO pass (feed pH = 9.6) as a function of recovery ratio .Squares are experimental results. Triangles are values predicted by the manufacturer software for feed pH 9.6 (black) and 7 (grey). Dashed lines are the projections by the fully functional *WATRO* model at feed pH 9.6 (black) and 7 (grey). Dotted line represents simulation results made by the modified version of *WATRO* with no H^+/OH^- flux

4.3. Implications on potential membrane scaling

The improved descriptions of the retentate pH has significant implications for the assessment of membrane scaling potential by minerals whose saturation state and precipitation potentials depend on pH. Table 4 shows the effect of projected brine pH on the scaling tendency of the most "problematic" minerals. When the pH of seawater brines was assumed equal to that of the feed (constant pH assumption) saturation indices and precipitation potentials are significantly higher compared to the more realistic lower pH prediction made by *WATRO*. Consequently, the induction time for nucleation is expected to be longer while crystal growth is expected at a lower rate. For the case of the 2nd pass brine (feed pH = 9.6), due to the high pH projected by the manufacturer software (pH10.5) compared to the much lower pH (pH8.77) projected by *WATRO* (closely matching experimental results), the calculated saturation state shifted from supersaturation to undersaturation (for brucite) or close to saturation (for calcite). These results imply that the use of antiscalants can be considerably reduced and even abandoned in certain cases, which is already practiced in many SWRO facilities however a sound mechanistic explanation has not been suggested until now.

Table 4. saturation indices (SI) and precipitation potentials (PP) for aragonite ($CaCO_3$) in seawater brines[38,39] and calcite ($CaCO_3$) plus brucite ($Mg(OH)_2$) in the 2nd pass brine[2]. Chemical equilibrium calculations were made with PHREEQC (Pitzer database). C_T stands for total inorganic carbon concentration.

Feed pH	brine pH	C_T (mmol/ kgH_2O)	Alkalinity (meq/ kgH_2O)	SI	PP (mg_$CaCO_3$/l)
	1st pass 50% recovery			Aragonite	Aragonite
8.15	8.15 (constant pH)	4.6	5.34	1.03	86.2
8.15	7.95 (*WATRO prediction*)	4.6	5.07	0.85	62.3
8.6	8.6 (constant pH)	4.6	6.27	1.38	170.5
8.6	8.37 (*WATRO prediction*)	4.6	5.73	1.21	121.8
	2nd pass 85% recovery			Calcite / Brucite	Calcite / Brucite
9.6	10.5 (Manufacturer software)	1.13	1.94	1.03 / 0.65	29.2 / 18.8
9.6	8.77 (WATRO prediction)	1.13	1.23	0.01 / -2.77	0.1 / -42.0

5. Conclusions

Overall, the model evaluation results demonstrate the applicability of the *WATRO* program for predicting pH, alkalinity and boron in SWRO for a range of feed pH values, different membranes and distinct feed compositions and pressure (1st pass versus 2nd pass). It was shown that pH variations in the retentate of the 1st SWRO pass operating at feed pH >8 are governed by the increase in salt concentration, while the permeate pH is mainly determined by the passage of hydronium and hydroxide ions through the membrane. The latter phenomenon was found to have a dramatic effect on both permeate and retentate pH in the 2nd pass, which explained the large discrepancies between measured results and projection by the manufacturer software. The mass transfer coefficient for boric acid was found to be significantly higher than that of the background salt, despite having similar diffusion coefficients. This observation calls for additional work focusing on the effect of solute charge on concentration polarization. Applying this modeling approach for SWRO could enable optimized boron removal while avoiding chemical scaling, thus resulting in a more cost-effective desalination process.

Acknowledgements

This project was funded by the Israel Science Foundation (#163/14).

References

1 P. Schausberger, G. M. Mustafa, G. Leslie and A. Friedl, *Desalination*, 2009, **244**, 31–47.

2 O. Nir, M. Herzberg, A. Sweity, L. Birnhack and O. Lahav, *Chem. Eng. J.*, 2012, **187**, 275–282.

3 A. Antony, J. H. Low, S. Gray, A. E. Childress, P. Le-Clech and G. Leslie, *J. Memb. Sci.*, 2011, **383**, 1–16.

4 C. E. Milstead, A. B. Riedinger and H. K. Lonsdale, *Desalination*, 1971, **9**, 217–223.

5 K. L. Tu, L. D. Nghiem and A. R. Chivas, *Sep. Purif. Technol.*, 2010, **75**, 87–101.

6 J.-J. Qin, M. H. Oo and B. Coniglio, *Desalination*, 2005, **177**, 267–272.

7 T. Waly, M. D. Kennedy, G.-J. Witkamp, G. Amy and J. C. Schippers, *Desalination*, 2011, **280**, 27–32.

8 O. Nir and O. Lahav, *Desalination*, 2013, **310**, 87–92.

9 O. Nir and O. Lahav, *Desalination*, 2014, **343**, 147–153.

10 O. Nir, E. Marvin and O. Lahav, *Water Res.*, 2014, **64**, 187–195.

11 O. Nir, N. F. Bishop, O. Lahav and V. Freger, *Water Res.*, 2015.

12 X. Cai, H. P. Langtangen and H. Moe, *Sci. Program.*, 2005, **13**, 31–56.

13 D. L. Parkhurst and C. A. J. Appelo, 1999.

14 S. R. Charlton and D. L. Parkhurst, *Comput. Geosci.*, 2011, **37**, 1653–1663.

15 A. Yaroshchuk, X. Martínez-Lladó, L. Llenas, M. Rovira and J. de Pablo, *J. Memb. Sci.*, 2011, **368**, 192–201.

16 J. G. Wijmans and R. W. Baker, *J. Memb. Sci.*, 1995, **107**, 1–21.

17 J. Wang, D. S. Dlamini, A. K. Mishra, M. T. M. Pendergast, M. C. Y. Wong, B. B. Mamba, V. Freger, A. R. D. Verliefde and E. M. V Hoek, *J. Memb. Sci.*, 2014, **454**, 516–537.

18 K. S. Pitzer, *J. Phys. Chem.*, 1973, **77**, 268–277.

19 C. E. Harvie and J. H. Weare, *Geochim. Cosmochim. Acta*, 1980, **44**, 981–997.

20 C. E. Harvie, N. Møller and J. H. Weare, *Geochim. Cosmochim. Acta*, 1984, **48**, 723–751.

21 L. N. Plummer, D. L. Parkhurst, G. W. Flemming and S. A. Dunkle, *A computer program incorporating Pitzer's equations for calculation of geochemical reactions in brines*, 1988, vol. 88-4153.

22 C. A. J. Appelo, *Appl. Geochemistry*, 2015, **55**, 62–71.

23 M. Azaroual, C. Kervévan, M. N. Durance and P. Durst, *Desalin. Strateg. South Mediterr. Ctries.*, 2004, **165**, 409–419.

24 K. H. Mistry, H. A. Hunter and J. H. Lienhard V, *Desalination*, 2013, **318**, 34–47.

25 H. Qian, Z. Zhou, L. Zhang, F. Wu, Q. Zhang and Z. Zhang, *Desalination*, 2013, **320**, 73–79.

26 T. H. Chong, F. S. Wong and A. G. Fane, *J. Memb. Sci.*, 2007, **287**, 198–210.

27 M. Fernanda Chillón Arias, L. V. i. Bru, D. P. Rico and P. V. Galvañ, *J. Memb. Sci.*, 2011, **368**, 86–94.

28 P. P. Mane, P.-K. Park, H. Hyung, J. C. Brown and J.-H. Kim, *J. Memb. Sci.*, 2009, **338**, 119–127.

29 S. Bason and V. Freger, *J. Memb. Sci.*, 2010, **360**, 389–396.

30 L. Ophek, L. Birnhack, O. Nir, E. Binshtein and O. Lahav, *Water Res.*, 2015, **85**, 185–192.

31 B. Andrews, B. Davé, P. López-Serrano, S.-P.-P. Tsai, R. Frank, M. Wilf and E. Koutsakos, *Eur. Desalin. Soc. Cent. Res. Technol. Hellas (CERTH), Sani Resort 22 –25 April 2007, Halkidiki, Greece Eur. Desalin. Soc. Cent. Res. Technol. Hellas (CERTH), Sani Resort*, 2008, **220**, 295–304. doi:10.1016/j.desal.2007.02.041

32 E. Mitsoyannis and G. D. Saravacos, *Desalination*, 1977, **21**, 235–240.

33 S. Oren, L. Birnhack, O. Lehmann and O. Lahav, *Sep. Purif. Technol.*, 2012, **89**, 252–260.

34 P.-K. Park, S. Lee, J.-S. Cho and J.-H. Kim, *Water Res.*, 2012, **46**, 3796–3804.

35 K. M. Sassi and I. M. Mujtaba, *J. Memb. Sci.*, 2013, **440**, 29–39.

36 S. Y. Alnouri and P. Linke, *Desalination*, 2014, **345**, 112–127.

37 O. Nir and O. Lahav, in *Boron Separation Processes*, ed. N. K. B. Hilal, Elsevier, Amsterdam, 2015, pp. 297–323.

38 J. W. Morse, Q. Wang and M. Y. Tsio, *Geology*, 1997, **25**, 85–87.

39 W. Sun, S. Jayaraman, W. Chen, K. A. Persson and G. Ceder, *Proc. Natl. Acad. Sci. U. S. A.*, 2015, **112**, 3199–204.

WATRO: *Weak Acids Transport Reverse Osmosis*

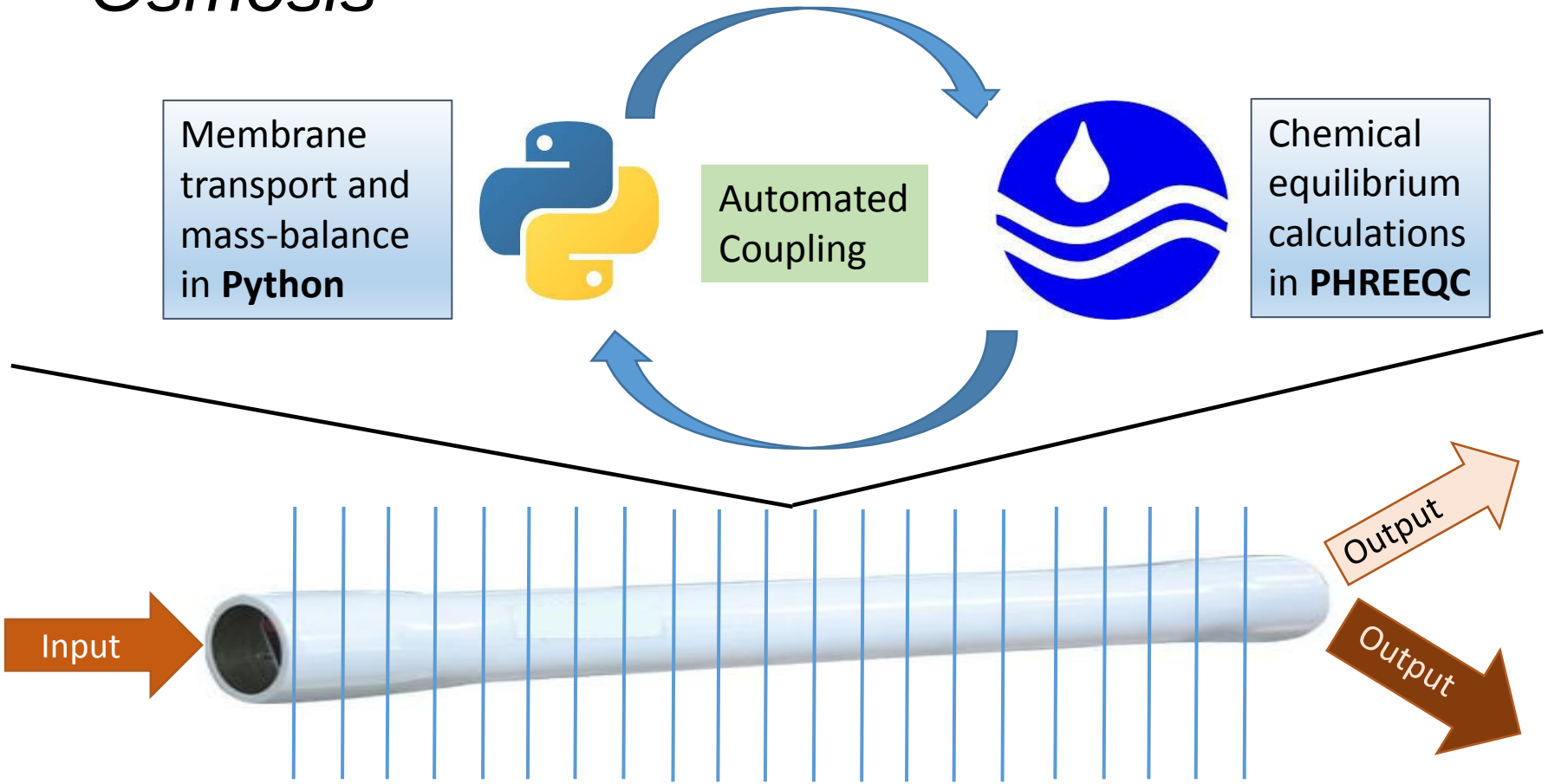

Advanced simulation algorithm enabling accurate predictions of acid-base properties in RO brine and permeate was developed and experimentally tested.